Tunneling in Unimolecular and Bimolecular Reactions

3

Hua Guo, Jianyi Ma, and Jun Li

Abstract

Tunneling is an important quantum phenomenon in reaction dynamics. In this chapter, the effects of tunneling on photodissociation and reactive scattering are discussed using two prototypical examples. The first deals with a unimolecular decomposition reaction, namely the photodissociation of NH_3 in its first (A) absorption band and the second is concerned with an important bimolecular reaction in combustion: $HO + CO \rightarrow H + CO_2$. In the former case, the lifetimes of low-lying vibrational resonances in the predissociative excited state are influenced by tunneling through a small barrier in the dissociation (N–H) coordinate, which is also responsible for a strong H/D isotope effect. The latter, on the other hand, is affected by tunneling through a tight barrier in the exit channel primarily along the H–O dissociation coordinate, which is manifested by the non-Arrhenius rate constant at low temperatures, kinetic isotope effects, and vibrational mode selectivity. In addition, the photodetachment of $HOCO^-$ produces metastable HOCO species, the decomposition of which is dominated by deep tunneling to the $H + CO_2$ products. Since both systems are influenced by multidimensional tunneling, an accurate characterization of the dynamics requires a quantum mechanical (QM) treatment, preferably with full dimensionality. In this chapter,

H. Guo (✉) • J. Li
Department of Chemistry and Chemical Biology, University of New Mexico, Albuquerque, NM 87131, USA
e-mail: hguo@unm.edu; junli11@unm.edu

J. Ma
Department of Chemistry and Chemical Biology, University of New Mexico, Albuquerque, NM 87131, USA

Institute of Atomic and Molecular Physics, Sichuan University, Chengdu, Sichuan 610065, China
e-mail: jianyi.m@gmail.com

F. Gatti (ed.), *Molecular Quantum Dynamics*, Physical Chemistry in Action,
DOI 10.1007/978-3-642-45290-1_3, © Springer-Verlag Berlin Heidelberg 2014

we review the recent advances in understanding the effects of tunneling in these two reactive systems.

3.1 Introduction

Tunneling is an important quantum effect, which stems from the particle-wave duality in quantum mechanics. A light quantum particle, which has a long de Broglie wavelength, is capable of having substantial non-zero probability amplitudes in classically forbidden regions. For many chemical reactions that possess a reaction barrier, for example, tunneling facilitates reactivity by penetrating the barrier at energies below the barrier height [1, 2]. Tunneling manifests in many observables such as non-Arrhenius behaviors of thermal rate constants at low temperatures and kinetic isotope effects, but an unambiguous and precise quantification of tunneling is not always straightforward for bimolecular reactions since the classical limit without tunneling is difficult to define. Tunneling is particularly facile if the reaction coordinate involves the motion of light atoms, such as hydrogen. A good example is the $H + H_2$ reaction [3], which has been shown by accurate quantum reactive scattering and transition-state theory calculations to exhibit strong non-Arrhenius effects at low temperatures and large kinetic isotope effects [4–6], thanks to tunneling as well as other quantum effects such as zero-point energy and resonances. The enhancement of the rate constant relative to the Arrhenius prediction at low temperatures is a tell-tale sign of tunneling, as it reduces the effective reaction barrier.

Since it is a quantum effect, a proper account of tunneling dynamics requires a QM treatment. While such a treatment has become routine for bound-state calculations in small polyatomic systems [7, 8], an accurate description of the tunneling affected reaction dynamics is much more difficult [9–11]. Apart from the exponential scaling of the number of degrees of freedom, the other main obstacles include the lack of an optimal coordinate system to describe the both reactant and product arrangement channels, the involvement of a large phase space, and the possible long lifetime when a reaction intermediate is involved. In addition, reliable multidimensional global potential energy surfaces (PESs) are often scarce, which prevent accurate QM calculations of the dynamics. Despite these challenges, significant progress has been made in QM treatments of tunneling and reaction dynamics in polyatomic reactive systems. In this chapter, we will focus on the role of tunneling in chemical reactions using two prototypical examples. The first is a unimolecular decomposition process, which involves the predissociation of ammonia (NH_3) in its first excited electronic state. The other is concerned with a bimolecular reaction: $HO + CO \rightarrow H + CO_2$, which plays an important role in many gas phase environments. These two prototypical systems share some important features. First, with six internal degrees of freedom these tetra-atomic systems offer much richer dynamics than the extensively studied triatomic reactions, but are more challenging to study quantum mechanically. Second and more relevant

to this chapter, the dynamics of these bond breaking and forming processes are significantly affected by tunneling.

3.2 Photodissociation of NH_3

The photo-induced dissociation of NH_3 to $NH_2(\tilde{A})/NH_2(\tilde{X}) + H$ has served as a prototype for understanding photodissociation dynamics in polyatomic systems [12, 13]. The first (A) absorption band between 45,000 and 67,000 cm^{-1} consists of a long series of nearly equidistant diffuse peaks, which have been assigned to excitations in the umbrella (2^n) vibration [14–16]. This progression reflects the dramatic change from the trigonal pyramidal (C_{3v}) equilibrium geometry of NH_3 in the ground electronic ($\tilde{X}^1A_1'$) state to the trigonal planar (D_{3h}) structure on the first excited electronic ($\tilde{A}^1A_2''$) state. The diffuse nature of the peaks suggests strong predissociation and the widths of these metastable resonances have been measured by many authors [17–24]. It was found that the line width, which is inversely proportional to the lifetime, of these vibrational levels depends on the vibrational quantum number (n). In addition, the widths of the ND_3 peaks are significantly narrower than their NH_3 counterparts, strongly suggesting tunneling.

The predissociation of ammonia stems from the quasi-bound nature of the vibrational states in the Franck–Condon region of the $\tilde{A}$-state PES. Ab initio calculations indicated a small barrier along the dissociation (N–H) coordinate immediately outside the Franck–Condon region [25–27], due primarily to the interaction between the N(3s) Rydberg state and the σ^* antibonding state. The existence of this barrier is consistent with the diffuse nature of the 2^n peaks and with the isotope effect, as the predissociation, at least for low energies, proceeds via tunneling. At higher energies, the lifetime is presumably influenced by a number of other factors, including intramolecular vibrational energy redistribution (IVR) among the various vibrational modes in NH_3. Beyond the barrier, the excited $\tilde{A}$-state forms a seam of conical intersections with the ground $\tilde{X}$-state [25–29], which are responsible for non-adiabatic transitions leading to the dominant $NH_2(\tilde{X}) + H$ fragmentation channel observed in experiment. The schematic $\tilde{X}/\tilde{A}$ PESs for ammonia are illustrated in Fig. 3.1.

The quasi-bound nature of $NH_3(\tilde{A}^1A_2'')$ in the Franck–Condon region provides an ideal case for studying tunneling dynamics in unimolecular reactions [27, 30–33]. As expected, the lifetime of a metastable quantum resonance state depends sensitively on the shape and height of the barrier, as well as other factors such as intermodal coupling. Indeed, the measured lifetimes of both NH_3 and ND_3 exhibit some surprising trends. For example, the first overtone of the umbrella vibration (2^1) of both NH_3 and ND_3 has a longer lifetime than the ground vibrational state (2^0) and the second overtone (2^2), although higher overtones typically have shorter lifetimes [15–17, 19, 22]. In order to quantitatively understand the unique dissociation dynamics, much effort has been devoted to the accurate determination of the PES of the excited as well as the ground states of NH_3 [25–29, 34]. However, it is only recently that ab initio-based full-dimensional PESs have become available.

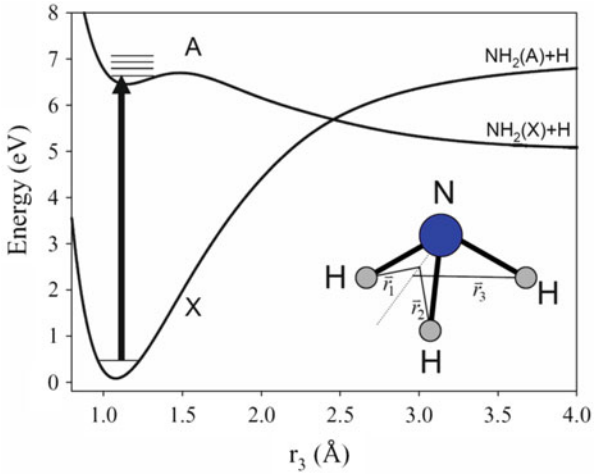

Fig. 3.1 Schematic $\tilde{X}/\tilde{A}$ potential energy surfaces for NH_3. Adapted from [38] with permission

To this end, Truhlar and coworkers have developed the first full-dimensional quasi-diabatic representation of the coupled $\tilde{X}/\tilde{A}$ PESs for NH_3 [35, 36]. More recently, Zhu, Ma, Guo, and Yarkony (ZMGY) presented a more accurate set of coupled quasi-diabatic PESs for this system [37]. These PESs allowed full-dimensional QM calculations of the absorption spectra, which yielded detailed information about the tunneling dynamics in this system [37–40].

Accurate knowledge of the PESs alone is of course insufficient to yield lifetimes. A QM treatment of the dissociation dynamics is required and full dimensionality is preferred as both tunneling and IVR are multidimensional in nature. To this end, we have developed such a wave packet-based method for the photodissociation of ammonia using an exact Hamiltonian ($J = 0$) for the nuclear motion [38]. The six-dimensional Hamiltonian and wavefunction in the Radau–Jacobi coordinates were discretized using a mixed representation [41]. Our approach relied on the Chebyshev propagation [42] of the excited state wave packet prepared by a vertical excitation from the ground electronic state, in the same spirit as the time-dependent approach to photodissociation [43]. The absorption spectrum can be readily obtained by a discrete Fourier transform of the Chebyshev autocorrelation function [44]. We note in passing that classical models have been employed for studying the photodissociation of ammonia [45, 46], but they are incapable of giving a good representation of the tunneling dynamics that dominates the absorption spectra.

The absorption spectra for both NH_3 and ND_3 were first calculated by our group [38] on the coupled full-dimensional PESs developed by Li, Valero, and Truhlar (LVT) [36]. Consistent with experiment, the absorption spectra are dominated by the predissociative umbrella (2^n) resonances. The calculated positions, widths, and intensities of these states are in qualitatively good agreement with the experimental

findings. For example, the ND_3 peaks have typically much narrower widths due to the larger reduced mass in the dissociation coordinate, consistent with the experimental observations [16, 17, 19]. Quantitatively, however, the line widths of the 2^n features in the absorption spectra, which underscore the state-specific tunneling rates, deviate significantly from the most reliable experimental values [34]. Specifically, the calculated widths of the low-lying states are generally three times too large, presumably because the classical barrier height of 1,750 cm^{-1} on the $\tilde{A}$-state PES [36] is too low compared with that estimated from experimental data ($\sim$2,100 cm^{-1}) [22]. Despite these large deviations, the 2^1 anomaly was reproduced. This anomaly is due apparently to the fact that the dissociation barrier rises quickly with the umbrella angle. Consequently, the 2^1 state, which has a node at planarity, is subjected to a larger effective barrier than the planar 2^0 state, thus possessing a longer lifetime [18]. For higher overtones, the predissociation is dominated by intermodel coupling, and as a result the dissociation rate increases with energy. Subsequent calculations by Giri et al. [39] using an approximate QM method yielded qualitatively similar results.

Since the nuclear dynamics was treated exactly, the errors in the absorption spectra can be attributed to inaccuracies in the PESs. Not surprisingly, the agreement with experiment is greatly improved when the more accurate ZMGY PESs were used [37]. In Fig. 3.2, the calculated absorption spectra of both NH_3 and ND_3 are compared with the experimental counterparts measured in a cold supersonic jet [19]. The nuclear spin statistics at the experimental temperature [26] has been included in the calculations. The agreement in both the positions and intensities is quite satisfactory. In addition, the calculated widths are also compared in Fig. 3.3 with experiment and previous theoretical results. The theory–experiment agreement in the absorption spectra is much better than that on the LVT PESs, and the agreement in the widths, including the 2^1 anomaly, is almost quantitative. The improvements can almost certainly be attributed to the higher level of the ab initio (multi-reference configuration interaction or MRCI using the aug-cc-pVTZ basis set with an extra 3 s Rydberg function for N) calculations and a better fitting scheme [47]. Indeed, the classical barrier height of the ZMGY $\tilde{A}$-state PES is, for example, 2,153 cm^{-1} [37], in much better agreement with the experimental estimation of $\sim$2,100 cm^{-1} [22].

It should be noted that the inclusion of the seam of conical intersections at larger N–H distances in latter dynamical calculations did not change the quantitative agreement in the absorption spectra [40], suggesting that the subsequent non-adiabatic dynamics has almost no impact on the initial tunneling dynamics. Interestingly, the ZMGY PESs have recently been shown to perform extremely well in reproducing the $NH_2(\tilde{A})/NH_2(\tilde{X})$ product branching ratio in the non-adiabatic dynamics of ammonia photodissociation [40], which further confirms the accuracy of the global PESs and their coupling.

One of the more intriguing questions concerning the tunneling dynamics in ammonia photodissociation is the impact of vibrational excitation prior to the electronic transition. Crim and coworkers have examined the action spectra of such vibrationally mediated photodissociation processes in NH_3 and found drastically

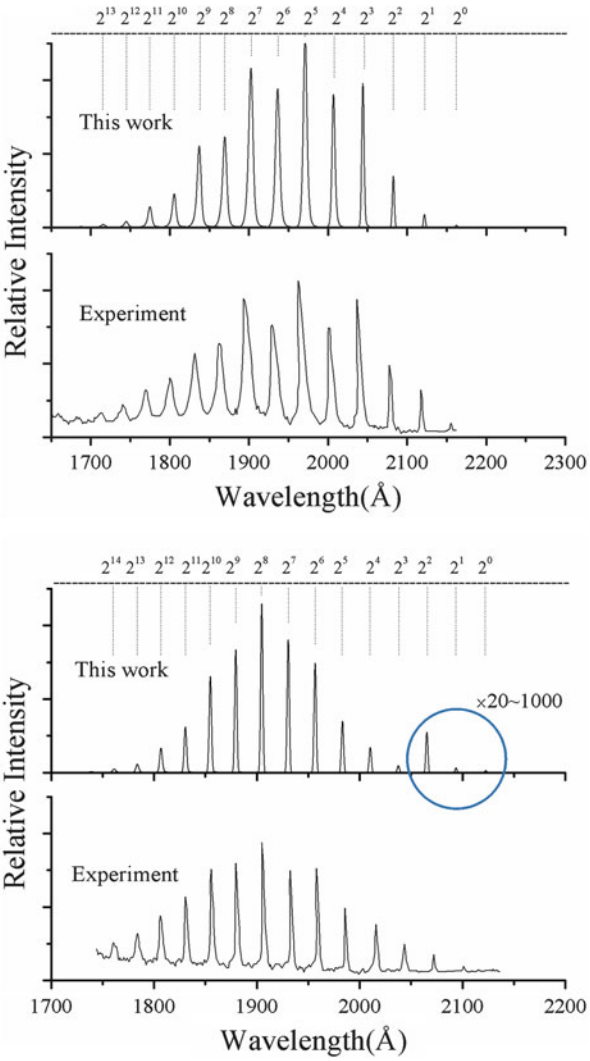

Fig. 3.2 Comparison of the calculated and measured [19] absorption spectra of NH_3 (*upper panel*) and ND_3 (*lower panel*). Adapted from [37] with permission

different line structures and widths from photodissociation of vibrationally unexcited NH_3 [34]. The changes in the absorption spectra can be qualitatively understood as different vibrational states on the ground electronic state have different Franck–Condon factors with those on the excited electronic $\tilde{A}$-state. More striking is the very unusual H translational energy distributions, which are interpreted as the result of changing product branching ratios resulted from different non-adiabatic transitions [48, 49]. Such problems can in principle be addressed using the same

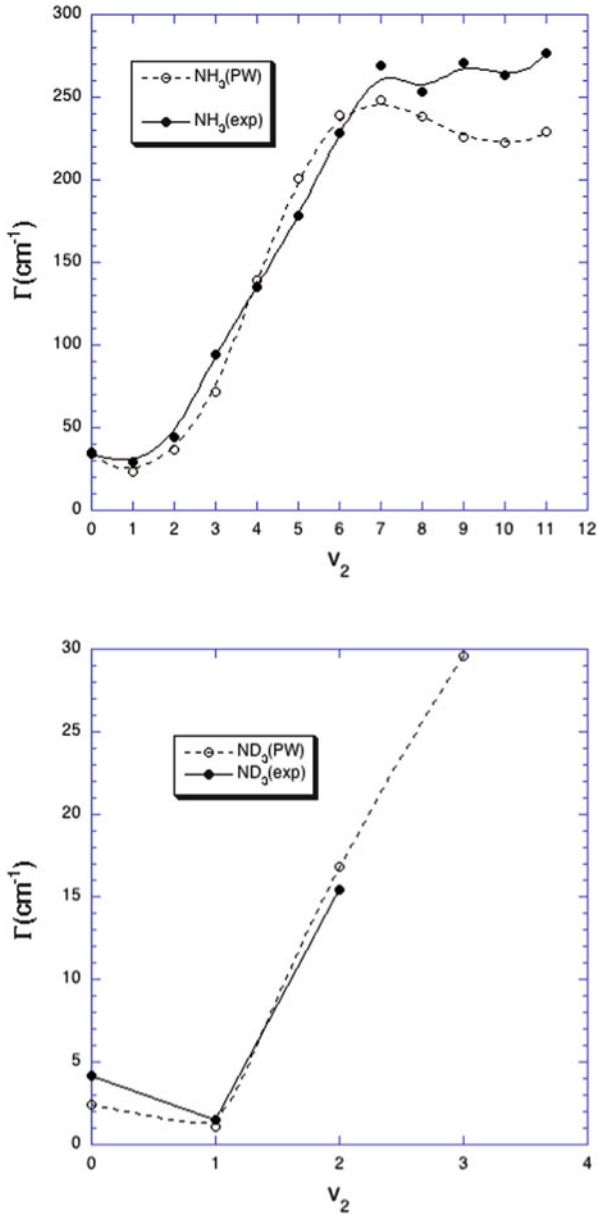

Fig. 3.3 Comparison of the calculated and measured [17, 19, 22] widths of the 2^n resonances of NH_3 (*upper panel*) and ND_3 (*lower panel*) in their absorption spectra. Adapted from [37] with permission

technique described above, which will provide additional information about the role of tunneling in this prototypical system.

3.3 $OH + CO \rightarrow H + CO_2$ Reaction

The exothermic OH + CO reaction plays an important role in combustion as the last step of hydrocarbon oxidation, which represents the main heat release step, and is considered to be the "second most important combustion reaction" [50]. It is also the main CO oxidation channel in the atmosphere and controls the atmospheric OH concentration [51]. Unlike many activated reactions, the PES of this reaction has a very small or null overall barrier. Instead, the association of HO and CO results in a relatively stable HOCO intermediate [52, 53], which has both *cis* and *trans* isomers. The kinetics of the reaction has been extensively studied and the rate constants have some very unusual characteristics [54–58]. For example, the reaction shows a strong pressure dependence, which was attributed to the complex-forming mechanism [54]. In addition, the rate constant is almost constant at low temperatures, but it increases sharply with temperature above 500 K. This non-Arrhenius behavior is indicative of tunneling along the reaction pathway. The importance of tunneling in the reaction dynamics is also supported by a strong H/D kinetic isotope effect [58–60], and rate enhancement *via* vibrational excitation of the OH reactant [59, 61, 62]. Indeed, tunneling has to be included in kinetic modeling of the reaction if a quantitative agreement with experiment is to be obtained [58, 63–65]. In particular, we note the recent semi-classical transition-state theory study of the reaction rate constant based on high-quality ab initio anharmonic force fields at transition states reproduced the experimental data, including the non-Arrhenius behaviors at low temperatures, almost perfectly [66], underscoring the importance of tunneling in the reaction.

This reaction and its reverse have become a prototype to understand complex-forming elementary reactions [9, 10, 67]. As illustrated in the previous section, the accuracy of the underlying PES is essential for quantitatively characterization of the reaction dynamics. For HOCO, several earlier global PESs, notably the ones by Schatz, Fitzcharles, and Harding (SFH) [68], by Yu, Muckerman, and Sears (YMS) [69], by Lakin, Troya, Schatz, and Harding (LTSH) [70], and by Valero, van Hemert, and Kroes (VvHK) [71], have been developed. These and other PESs have been used in numerous dynamical calculations, using both quasi-classical trajectory (QCT) [68, 70, 72–81] and QM methods [82–99]. Unfortunately, these PESs do not have the necessary accuracy, due primarily to the small number of ab initio points used in constructing these six-dimensional potential energy functions. To improve our understanding of this important reactive system, we have recently reported a new global PES for this system at the level of UCCSD(T)-F12/AVTZ [100–102]. This represents the most accurate level of theory affordable at present and the accuracy has recently been corroborated by MRCI + Q-F12 calculations [103]. Approximately ~50,000 points distributed in a large configuration space relevant to the reaction were fit with the permutation invariant polynomial method [104, 105]. The PES represents the stationary points

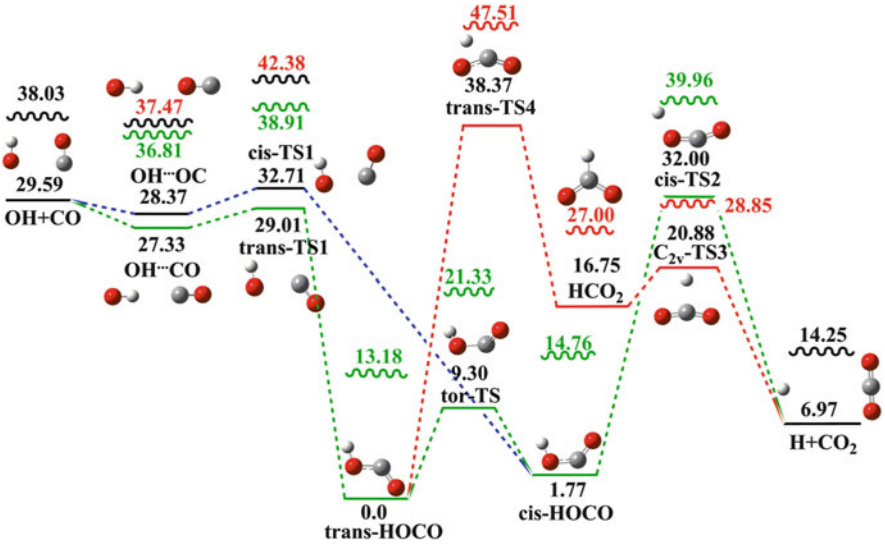

Fig. 3.4 Energetics of reaction pathways for the $HO + CO \rightarrow H + CO_2$ reaction. The ab initio energies (E_0) of the stationary points are given in kcal/mol relative to the *trans*-HOCO minimum. The wavy lines are for ZPE-corrected energies ($E_0 + ZPE$) of the relevant species. All species are planar, except tor-TS. Adapted with permission from [101]

quite well with a global fitting error of roughly 1.0 kcal/mol, indicating that the PES is sufficiently accurate for most dynamical calculations.

The ab initio-based energetics of the reaction pathway for this reaction is illustrated in Fig. 3.4. From the $HO + CO$ reactants, two pathways exist for the formation of the HOCO intermediate, each gated by a bottleneck (*trans* or *cis*-TS1). In the entrance channel, there also exist two collinear hydrogen-bonded van der Waals complexes, one of which has been detected experimentally [106]. Within the HOCO well, the *cis* and *trans*-HOCO species are separated by a relatively low isomerization barrier (tor-TS). On the other hand, the dissociation of the two HOCO isomers to the $H + CO_2$ products is controlled by two other transition states, namely TS2 and TS4, with the latter less relevant at low collision energies due to its higher energy. A key feature of the HOCO PES is that the lowest entrance and exit barriers are roughly isoenergetic, which give rise to the unusual kinetic behaviors of the reaction discussed above. In particular, the exit channel transition state (TS2) is much tighter and has a reaction coordinate dominated by the H–O stretching motion, which is amenable to tunneling dynamics.

This new PES was used in a recent full-dimensional QM calculations [107], which solves the nuclear Schrödinger equation with the Chebyshev propagator [42] in the OH–CO Jacobi coordinates. Such calculations are extremely challenging due to the three heavy atoms in the system and the large number of quantum states supported by the HOCO well. As a result, only the $J = 0$ partial wave was considered. The initial state in the reactant asymptote was represented by a

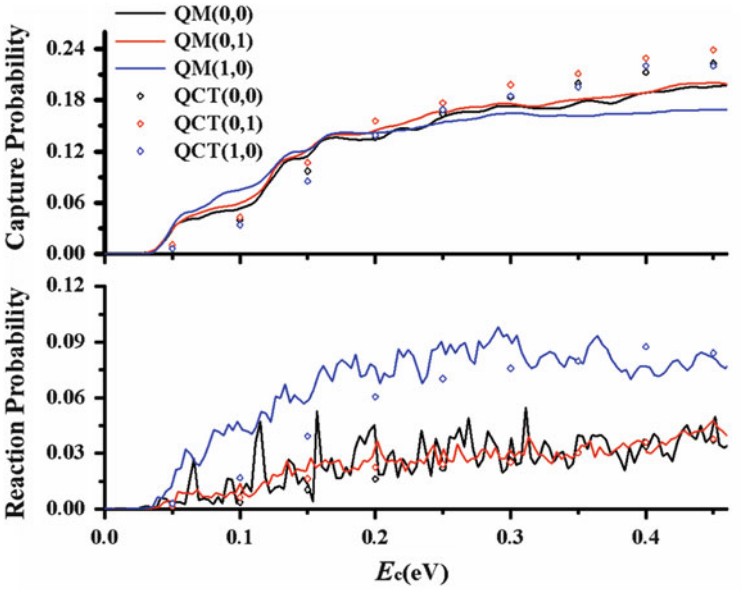

Fig. 3.5 Capture (*upper panel*) and reaction (*lower panel*) probabilities ($J = 0$) for (n_{OH}, n_{CO}) states of reactants as a function of collision energy (E_c). The quantum mechanical (QM) and QCT results ($b = 0$) are given in lines and symbols, respectively. Adapted with permission from [107]

Gaussian wave packet in the scattering coordinate multiplied by the internal state wave functions for OH and CO. A mixed grid/basis representation [41] was used to discretize the Hamiltonian and wave packet. The energy-dependent total reaction probability was calculated using a flux method [108] at a dividing surface placed in the product channel just beyond TS2. For capture calculations, on the other hand, the dividing surface was placed behind TS1, which saves a large number of grid points. The calculated $J = 0$ capture and reaction probabilities for a number of reactant internal states are shown in Fig. 3.5 as a function of the collision energy. As comparison, corresponding QCT results were also obtained with zero impact parameter ($b = 0$) and included in the same figure. It is clear from the figure that the reactivity is very low despite its near barrierless nature, in qualitative agreement with previous QM calculations on earlier PESs [93, 94, 98]. This is due to the fact that the reaction has to overcome two bottlenecks in both the entrance and exit channels, as shown by the substantially larger capture probabilities in Fig. 3.5. Both the capture and reaction probabilities tend to increase with the collision energy with a common reaction threshold of ~0.03 eV, which is primarily due to the entrance channel bottleneck. The oscillatory structures in the reaction probabilities are apparently due to numerous overlapping resonances, which have been noted in previous QM calculations [93, 94, 98].

As shown in Fig. 3.5, excitation in the vibration of the OH reactant ($v = 1$) significantly enhances the reactivity, while the effect in CO excitation is limited.

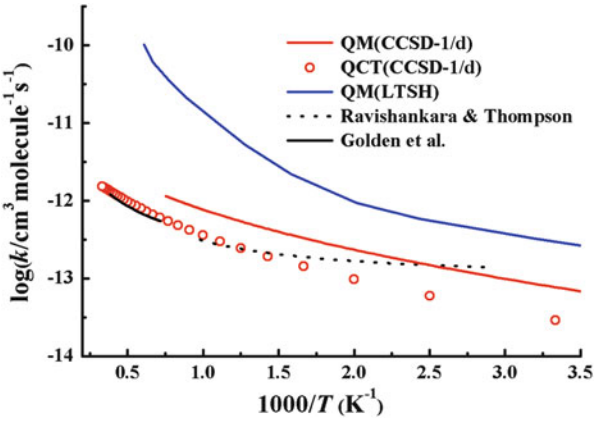

Fig. 3.6 Comparison of calculated quantum and QCT rate constants with experimental ones in the low pressure limit [55, 58]. The quantum rate constants reported by Liu et al. [98] on the LTSH PES are also included for comparison. Adapted with permission from [107]

This observation is consistent with experimental evidence for this reaction [59, 61], as well as our earlier QCT work [101] and previous QM calculations on the LTSH PES [98, 99]. Interestingly, the vibrational excitation in the reactant has little impact on the capture probabilities. This follows that the energy imparted in the OH vibration helps to surmount TS2 as the reaction coordinate at the saddle point is essentially the O–H stretch. However, this is possible only when the HOCO intermediate is relatively short-lived, rendering incomplete randomization of energy before surmounting TS2, which retains energy in the O–H bond. A short-lived HOCO intermediate is consistent with experimental observations [52, 53, 109, 110] and our QCT studies of this system on this new PES [101, 102].

It is also interesting to compare the $J = 0$ capture and reaction probabilities with the corresponding QCT results obtained with zero impact parameter. Although the QCT probabilities cannot account for quantum resonances, Fig. 3.5 suggests that the overall agreement with the corresponding QM results is quite reasonable. The QCT probabilities are typically smaller than their quantum counterparts at lower collision energy, particularly for the OH excited case, suggestive of tunneling. The importance of tunneling is expected to be even more pronounced as J increases, because the tight TS2 saddle point is raised by the centrifugal potential.

Figure 3.6 displays the comparison of the theoretically calculated thermal rate constants with the experimental data in the low pressure limit [55, 58]. The QM rate constants were estimated using the J-shifting method [111] with energy shifts determined at TS2, while the standard thermal sampling was used in the QCT calculations [100]. A caveat is in order concerning the validity of the J-shifting approximation in complex-forming reactions, since the reactivity in such a reaction is not completely determined by the saddle point [67]. For comparison, the J-shifted QM rate constants reported by Liu et al. [98], who used the earlier LTSH PES [98],

are also included in the same figure. The calculated QM rate constants on the new PES are in much better agreement with experimental data than that obtained on the LTSH PES, although there is still significant underestimation at low temperatures and overestimation at high temperatures. The discrepancies at low temperatures are partially due to tunneling that is not completely captured by the J-shifting model. Indeed, the centrifugal potential for $J > 0$ is expected to raise the thin barrier at the tight TS2 saddle point to energies significantly higher than the reactant asymptote, further accentuating the impact of tunneling. On the other hand, the errors at high temperatures may also be due to the over-simplification of the J-shifting model, but the precise origin has to await future explicit $J > 0$ calculations. Since the same QM method was used, the improvement in the theory–experiment agreement for thermal rate constants can be attributed to the improved accuracy in the new PES. On the other hand, the QCT rate constants also reproduced the high temperature data quite well, but underestimate at low temperatures, due almost certainly to the neglect of tunneling.

Despite the improvements in describing the reaction PES for the $HO + CO \rightarrow H + CO_2$ reaction, there is evidence indicating that the new PES is still not perfect. For example, our recent QCT studies [101, 112] failed to reproduce the experimental internal state distribution of the CO_2 product [109, 113, 114] and the corresponding angular distribution [80, 109, 114]. For the reverse $H + CO_2 \rightarrow HO + CO$ reaction, our QCT results [102] underestimate the CO rotational state distribution [115, 116], although in good agreement with the experimental rate constant [117], total integral cross sections [118, 119], and the HO rotational distribution [118, 119]. It is possible that these discrepancies are due to experimental errors, but it is more likely that subtle deficiencies in the PES are the culprit. Indeed, a more recent fit of the CCSD(T)-F12/AVTZ points for this system using neural network has uncovered several shortcoming of our PES, resulting in even lower reaction probabilities [120].

The most dramatic manifestation of tunneling was found in the photodetachment of the $HOCO^-$ anion, which produces the neutral HOCO species and its dissociation fragments. Photodetachment of negative ions has been widely used as a powerful way to probe dynamics of chemical reactions on the corresponding neutral PESs [121]. Since this approach sometimes affords a direct access to the transition-state region of the bimolecular reactions, this so-called transition-state spectroscopy by negative ion photodetachment has revealed intricate resonances near the reaction barrier [122], which control the reactivity. The photodetachment of $HOCO^-$ (and $DOCO^-$) has been extensively investigated by Continetti and coworkers [123–128]. The photo-ejection of an electron from the anion places the system on the neutral PES near the HOCO wells. Earlier photoelectron–photofragment coincidence (PPC) experiments revealed the formation of the HOCO, $HO + CO$, and $H + CO_2$ products [123, 124]. More recently, a new cryogenically cooled PPC apparatus was employed to achieve much higher resolution and to eliminate hot bands [126, 127]. One of the most striking observations is that nearly all photoelectrons in the $H + CO_2$ channel were found to have energies above the maximum limit predicted for TS2, suggesting the dissociation of HOCO into the $H + CO_2$ channel is mostly via tunneling through the barrier [126, 127]. In other words, the reaction is pure quantum in nature.

Interestingly, an earlier full-dimensional QM study of the photodetachment of $HOCO^-$ found no evidence of tunneling, although all three experimentally observed channels were identified [129]. There are several reasons for the discrepancy. The most likely is that the LTSH PES [70] used in the calculation was not sufficiently accurate, particularly with regard to the thickness of the barrier associated with TS2, as shown in our recent work [100, 101]. As a result, tunneling might be substantially underestimated. We have reinvestigated [130] the problem using our new HOCO PES [100, 101], which has a much thinner barrier leading to the $H + CO_2$ products than the LTSH PES. Both full-dimensional and reduced-dimensional QM models have been used. This is important because ample evidence suggests that tunneling is a multidimensional phenomenon [100, 127]. Due to the formidable computational costs, however, the former was restricted to the calculation of the low-resolution energy spectrum of the photodetachment, which is pertinent to the initial evolution of the wave packet on the neutral PES. In order to describe long time events due to tunneling, on the other hand, the dynamics was followed using a five-dimensional model with the non-reacting C–O bond fixed. While recent QM studies have shown that the non-reactive CO bond is not in the strict sense a spectator in the $HO + CO$ reaction [95, 98], this approximation is unlikely to qualitatively change the conclusion for photodetachment, especially concerning the tunneling over TS2. This is because the C–O bond length does not change significantly over the course of the dissociation.

The theoretical model for photodetachment is similar to that used to describe photodissociation outlined in the last section. As illustrated in Fig. 3.7, the initial wave packet on the neutral PES was chosen as the ground vibrational state of *cis*-$HOCO^-$, which has a lower energy than its *trans* counterpart. The anion vibrational eigenfunction was determined on a newly developed anion PES at the same CCSD(T)-F12/AVTZ level [130], as used to construct the neutral PES [100, 101]. The neutral wave packet was propagated to yield probabilities to both the $HO + CO$ and $H + CO_2$ asymptotes with a flux method [108] and the cosine Fourier transform of the Chebyshev autocorrelation function yielded the energy spectrum [44]. The discretization of the Hamiltonian and wavepacket, and the propagation were essentially the same as in our recent reaction dynamics study [107].

In Fig. 3.7, the low-resolution spectra were obtained from the Fourier transform of the corresponding Chebyshev autocorrelation functions after a short (100 steps) propagation of the initial wave packets on the neutral PES. In the same figure, we have also included the spectrum converted from the experimental electronic kinetic energy (eKE) distribution [126] via the following relation: $E = h\nu - \text{eKE}$, where the experimental photon energy is 3.21 eV (386 nm) [126]. The agreement between the experimental distribution and the full-dimensional spectrum is excellent, validating the PESs used in the calculations. The shift of the reduced-dimensional spectrum can presumably be attributed to the freezing of the non-reactive CO bond. It is interesting to note that the geometry of the anion is sufficiently similar to that of the corresponding neutral species, little amplitude was found outside the HOCO well on the neutral PES. This observation is important because it indicates that only a small

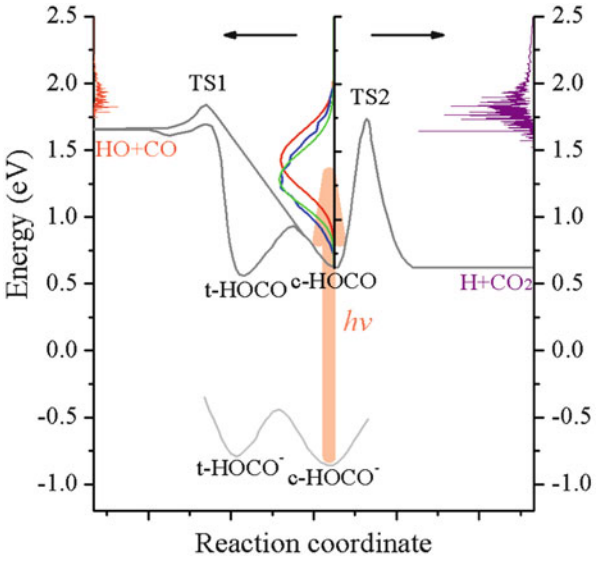

Fig. 3.7 Zero-point corrected energetics of the schematic HOCO/$HOCO^-$ PESs. The energy zero is placed at the global *trans*-HOCO minimum of the neutral PES. The calculated energy spectrum of the HOCO species prepared by photodetachment of the $HOCO^-$ anion is displayed in *green* (full-dimensional model) and *red* (five-dimensional model) with the experimentally derived spectrum in *blue*. In addition, the calculated dissociation probabilities for the HO + CO and $H + CO_2$ channels are also given in *orange* and *purple*. Note the substantial probabilities in the latter channel suggest tunneling. Adapted with permission from [130]

fraction of the neutral species will have the necessary energy to dissociate directly into both the HO + CO and $H + CO_2$ channels. On the other hand, the majority of the neutral species prepared by photodetachment is temporarily trapped in the HOCO well as metastable resonances. As shown in Fig. 3.4, the trapped HOCO species has no choice but to decay via tunneling through the barrier under TS2.

In Fig. 3.8, the high-resolution energy spectrum of HOCO prepared by photodetachment of *cis*-$HOCO^-$ is displayed. As expected, all HOCO species below the effective dissociation barriers exist as resonances, as illustrated by the sharp peaks in Fig. 3.8. There is no bound state because the lowest-lying vibrational state of *cis*-HOCO is above the $H + CO_2$ asymptote. Based on inspection of wave functions, these peaks can be assigned to bending (ν_5) progressions, due apparently to the fact that the bending angles of the anion differ significantly from those of the neutral species. Some excitation in the reactive C–O bond stretch (ν_4) is also present. On the other hand, the OH bond length in the negative ion and the neutral species is roughly the same, resulting in negligible excitation in ν_1 (O–H stretch). This assignment is in good agreement with the most recent photoelectron spectroscopic study of the cold $HOCO^-$ anion, in which bending progressions in ν_5 with some excitations in ν_4 and ν_3 (HOC bend) were found [128]. As discussed in our recent work [101], the vibrational frequencies of both *cis* and *trans*-HOCO species calculated on our PES

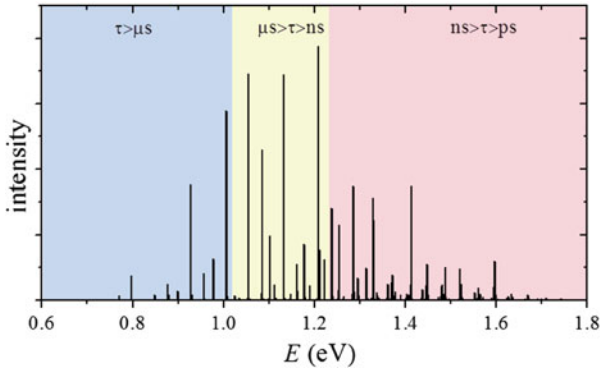

Fig. 3.8 High-resolution energy spectrum for HOCO prepared by photodetachment of the $HOCO^-$ anion. The energy is referenced to the *trans*-HOCO potential minimum and the approximate lifetime ranges of the resonances are color coded in *blue* for μs, *orange* for ns, and *red* for ps. Adapted with permission from [130]

are in good agreement with these experimental results as well as the benchmark ab initio data reported in the same publication [128].

The line widths of these resonances have been estimated and they are grouped in Fig. 3.8 based on their calculated lifetimes. It is clear that some of the resonances have exceedingly long lifetimes (>μs), which are comparable to the flight time in the experimental set up [127]. As a result, these resonances would have been classified as stable HOCO species in the experiment. Close to the energy of TS2, the lifetimes are on the order of ps, which can be readily captured in our flux calculations. The range of the lifetimes reported here is consistent with the estimates based on an earlier effective one-dimensional model [127]. Above the dissociation limit, there are still resonances superimposed on broad features, which correspond to direct dissociation.

The calculated dissociation probabilities to the HO + CO and H + CO_2 arrangement channels are shown in Fig. 3.7. In the HO + CO channel, the energy distribution centers at 1.82 eV relative to the *trans*-HOCO global minimum, in good agreement with the experimental distribution between 1.65 and 2.0 eV [126]. Comparing with the H + CO_2 channel, the HO + CO fraction is substantially smaller, again consistent with experiment [126]. On the other hand, the probability for the H + CO_2 channel has contributions from both above and under the TS2 barrier. The former converges quickly because of the relatively short time needed to dissociate. However, the tunneling contribution, which is apparent in the figure below the dissociation limit, is not quite converged in our calculation due to the extremely long lifetimes of the resonances at low energies. Nonetheless, it is clear that the tunneling channel makes up a large percentage of the total photodetachment.

In comparing with the experimental branching ratios, it is important to realize that the experimentally detected HOCO species are not strictly speaking stable because these resonances have energies higher than the H + CO_2 dissociation asymptote. However, lifetimes of these deep tunneling states are so long that the

7.8 μs flight time [127] might still be insufficient to observe their decomposition. As discussed above, it is impractical to expect wave packet propagations on such time scales either. Consequently, there is substantial uncertainty in the partition of the HOCO and $H + CO_2$ channels below the barrier. However, this uncertainty does not affect the overall agreement between theory and experiment. The calculation results presented here clearly demonstrated that photodetachment of $HOCO^-$ produces predominantly HOCO resonances that dissociate into $H + CO_2$, in agreement with the conclusion made by Continetti and coworkers [127].

Finally, it might be worthwhile to comment on the impact of tunneling facilitated HOCO decomposition in the bimolecular $HO + CO \rightarrow H + CO_2$ reaction kinetics. In the low pressure limit, the HOCO intermediate formed is largely above TS2 and as a result tunneling will be mostly through the centrifugal barrier near the exit bottleneck (TS2). In the high pressure limit, on the other hand, the reaction rate is dominated by the formation (capture) rate of the HOCO intermediate, as its overcome of the exit barrier is achieved by collisional excitations. The tunneling facilitated decomposition of thermalized HOCO is thus of less importance. As a result, the tunneling effect is expected to have an important, but not overwhelming, impact on kinetics of this bimolecular reaction and the impact will be limited to low temperatures.

3.4 Conclusions

In this chapter, we have shown through two examples the important role played by tunneling in reaction dynamics. In the unimolecular dissociation dynamics of ammonia photodissociation on its first excited electronic state, the lifetimes of the lowest-lying resonances are strongly affected by tunneling over a small barrier in the dissociation coordinate, which is responsible for a lifetime anomaly in the first overtone and for the large H/D isotope effect. Similarly, the tunneling in the bimolecular $HO + CO \rightarrow H + CO_2$ reaction has been shown to affect the rate constants at low temperatures as well as the H/D isotope effect. These two examples illustrate a typical scenario for the well-known quantum phenomenon in molecular systems, in which the dynamics is nominally perturbed by tunneling. On the other hand, chemical reactions dominated by deep tunneling are uncommon. In two systems found recently [131, 132], for example, the dominant products are produced via deep tunneling over a higher barrier even when another channel with a lower barrier is available. The photodetachment of $HOCO^-$ presents another interesting example, in which the decomposition of HOCO is almost exclusively due to tunneling. These unique reaction systems, suggest that quantum effects such as tunneling can in a few cases dominate, rather than merely influence, reactive systems.

Acknowledgments This work has been supported by the Department of Energy and National Science Foundation. We would also like to thank Joel Bowman, Fleming Crim, Richard Dawes, Evi Goldfield, Don Truhlar, Al Wagner, Daiqian Xie, David Yarkony, and Dong Hui Zhang for many stimulating discussions.

References

1. Schatz GC (1987) Tunneling in bimolecular collisions. Chem Rev 87:81
2. Schatz GC (1988) Quantum effects in gas phase bimolecular chemical reactions. Annu Rev Phys Chem 39:317
3. Aoiz FJ, Banares L, Herrero VJ (2005) The $H + H_2$ reactive system. Progress in the study of the simplest reaction. Int Rev Phys Chem 24:119
4. Mielke SL, Peterson KA, Schwenke DW, Garrett BC, Truhlar DG, Michael JV, Su M-C, Sutherland JW (2003) $H + H_2$ thermal reaction: a convergence of theory and experiment. Phys Rev Lett 91:063201
5. Fleming DG, Arseneau DJ, Sukhorukov O, Brewer JH, Mielke SL, Schatz GC, Garrett BC, Peterson KA, Truhlar DG (2011) Kinetic isotope effects for the reactions of muonic helium and muonium with H_2. Science 331:448
6. Suleimanov YV, Pérez de Tudela R, Jambrina PG, Castillo JF, Sáez-Rábanos V, Manolopoulos DE, Aoiz FJ (2013) A ring polymer molecular dynamics study of the isotopologues of the $H + H_2$ reaction. Phys Chem Chem Phys 15:3655
7. Guo H (2007) Recursive solutions to large eigenproblems in molecular spectroscopy and reaction dynamics. Rev Comput Chem 25:285
8. Bowman JM, Carrington T, Meyer H-D (2008) Variational quantum approaches for computing vibrational energies of polyatomic molecules. Mol Phys 106:2145
9. Bowman JM, Schatz GC (1995) Theoretical studies of polyatomic bimolecular reaction dynamics. Annu Rev Phys Chem 46:169
10. Althorpe SC, Clary DC (2003) Quantum scattering calculations on chemical reactions. Annu Rev Phys Chem 54:493
11. Nyman G, Yu H-G (2012) Quantum approaches to polyatomic reaction dynamics. Int Rev Phys Chem 32:39
12. Ashfold MNR, Bennett CL, Stickland RJ (1987) Rydberg states of ammonia. Comments At Mol Phys 19:181
13. Dixon RN (1994) Liversidge lecture. The dynamics of photodissociation. Chem Soc Rev 23:375
14. Leifson SW (1933) Astrophys J 63:73
15. Douglas AE (1963) Discuss Faraday Soc 35:158
16. Vaida V, Hess W, Roebber JL (1984) The direct ultraviolet absorption spectrum of the $A^1A_2'' \leftarrow X^1A_1$ transition of jet-cooled ammonia. J Phys Chem 88:3397
17. Ziegler LD (1985) Rovibrational absorption analysis of the A←X transition of ammonia. J Chem Phys 82:664
18. Ashfold MNR, Bennett CL, Dixon RN (1986) Dissociation dynamics of NH_3. Faraday Disc Chem Soc 82:163
19. Vaida V, McCarthy MI, Engelking PC, Rosmus P, Werner H-J, Botschwina P (1987) The ultraviolet absorption spectrum of the $A^1A_2'' \leftarrow X^1A_1'$ transition of jet-cooled ammonia. J Chem Phys 86:6669
20. Nakajima A, Fuke K, Tsukamoto K, Yoshida Y, Kaya K (1991) Photodissociation dynamics of NH_3, NH_2D, NHD_2, and ND_3: rovibronic absorption analysis of the A–X transition. J Phys Chem 95:571
21. Henck SA, Mason MA, Yan W-B, Lehmann KK, Coy SL (1995) Microwave detected, microwave-optical double resonance of NH_3, NH_2D, HND_2, and ND_3. I. Structure and force field of the A state. J Chem Phys 102:4772
22. Henck SA, Mason MA, Yan W-B, Lehmann KK, Coy SL (1995) Microwave detected, microwave-optical double resonance of NH_3, NH_2D, HND_2, and ND_3. II. Predissociation dynamics of the A state. J Chem Phys 102:4783
23. Baronavski AP, Owrutsky JC (1995) Lifetime of the $v_2' = 1$ A state of ND_3 measured by two color deep UV femtosecond multiphoton ionization spectroscopy. J Phys Chem 99:10077

24. Wells KL, Perriam G, Stavros VG (2009) Time-resolved velocity map ion imaging study of NH_3 photodissociation. J Chem Phys 130:074308
25. Runau R, Peyerimhoff SD, Buenker RJ (1977) Ab initio study of photodissociation of ammonia. J Mol Spectrosc 68:253
26. Rosmus P, Botschwina P, Werner H-J, Vaida V, Engelking PC, McCarthy MI (1987) Theoretical A–X absorption and emission spectrum of ammonia. J Chem Phys 86:6677
27. McCarthy MI, Rosmus P, Werner H-J, Botschwina P, Vaida V (1987) Dissociation of NH_3 to $NH_2 + H$. J Chem Phys 86:6693
28. Manz U, Reinsch E-A, Rosmus P, Werner H-J, O'Neil SV (1809) Dissociation of NH_3 to $NH + H_2$. J Chem Soc Faraday Trans 1991:87
29. Yarkony DR (2004) Exploring molecular complexity: conical intersections and NH_3 photodissociation. J Chem Phys 121:628
30. Dixon RN (1988) The stretching vibrations of ammonia in its A^1A'' excited state. Chem Phys Lett 147:377
31. Dixon RN (1996) Photodissociation dynamics of A state ammonia molecules. III. A three-dimensional time-dependent calculation using ab initio potential energy surfaces. Mol Phys 88:949
32. Tang SL, Imre DG (1988) Ammonia, the A<−X transition. Chem Phys Lett 144:6
33. Seideman T (1995) The predissociation dynamics of ammonia: a theoretical study. J Chem Phys 103:10556
34. Bach A, Hutchison JM, Holiday RJ, Crim FF (2002) Vibronic structure and photodissociation dynamics of the A state of jet-cooled ammonia. J Chem Phys 116:9315
35. Nangia S, Truhlar DG (2006) Direct calculation of coupled diabatic potential-energy surfaces for ammonia and mapping of a four-dimensional conical intersection seam. J Chem Phys 124:124309
36. Li ZH, Valero R, Truhlar DG (2007) Improved direct diabatization and coupled potential energy surfaces for the photodissociation of ammonia. Theor Chem Acc 118:9
37. Zhu X, Ma J, Yarkony DR, Guo H (2012) Computational determination of the A state absorption spectrum of NH_3 and of ND_3 using a new quasi-diabatic representation of the X and A states and full six-dimensional quantum dynamics. J Chem Phys 136:234301
38. Lai W, Lin SY, Xie D, Guo H (2008) Full-dimensional quantum dynamics of A-state photodissociation of ammonia. Absorption spectra. J Chem Phys 129:154311
39. Giri K, Chapman E, Sanz CS, Worth G (2011) A full-dimensional coupled-surface study of the photodissociation dynamics of ammonia using the multiconfiguration time-dependent Hartree method. J Chem Phys 135:044311
40. Ma J, Zhu X, Guo H, Yarkony DR (2012) First principles determination of the NH_2/ND_2(A/X) branching ratios for photodissociation of NH_3/ND_3 via full-dimensional quantum dynamics based on a new quasi-diabatic representation of coupled ab initio potential energy surface. J Chem Phys 137:22A541
41. Chen R, Ma G, Guo H (2001) Six-dimensional quantum calculation of highly excited vibrational energy levels of hydrogen peroxide and its deuterated isotopomers. J Chem Phys 114:4763
42. Chen R, Guo H (1996) Evolution of quantum system in order domain of Chebychev operator. J Chem Phys 105:3569
43. Balint-Kurti GG (2008) Time-dependent and time-independent wavepacket approaches to reactive scattering and photodissociation dynamics. Int Rev Phys Chem 27:507
44. Guo H (1998) A time-independent theory of photodissociation based on polynomial propagation. J Chem Phys 108:2466
45. Bonhommeau D, Truhlar DG (2008) Mixed quantum/classical investigation of the photodissociation of NH_3(A) and a practical method for maintaining zero-point energy in classical trajectories. J Chem Phys 129:014302
46. Bonhommeau D, Valero R, Truhlar DG, Jasper AW (2009) Coupled-surface investigation of the photodissociation of $NH_3(\tilde{A})$: effect of exciting the symmetric and antisymmetric stretching modes. J Chem Phys 130:234303

47. Zhu X, Yarkony DR (2012) On the representation of coupled adiabatic potential energy surfaces using quasi-diabatic Hamiltonians: a distributed origins expansion approach. J Chem Phys 136:174110
48. Bach A, Hutchison JM, Holiday RJ, Crim FF (2003) Competition between adiabatic and nonadiabatic pathways in the photodissociation of vibrationally excited ammonia. J Phys Chem A 107:10490
49. Hause ML, Yoon YH, Crim FF (2006) Vibrationally mediated photodissociation of ammonia: the influence of N–H stretching vibrations on passage through conical intersections. J Chem Phys 125:174309
50. Miller JA, Kee RJ, Westbrook CK (1990) Chemical-kinetics and combustion modeling. Annu Rev Phys Chem 41:345
51. Wayne RP (2000) Chemistry of atmospheres. Oxford University Press, Oxford
52. Scherer NF, Sipes C, Bernstein RB, Zewail AH (1990) Real-time clocking of bimolecular reactions: application to $H + CO_2$. J Chem Phys 92:5239
53. Ionov SI, Brucker GA, Jaques C, Valachovic L, Wittig C (1993) Subpicosecond resolution studies of the $H + CO_2 \rightarrow CO + OH$ reaction photoinitiated in CO_2–HI complexes. J Chem Phys 99:6553
54. Smith IWM, Zellner R (1973) Rate measurements of reactions of OH by resonance absorption. Part 2. Reaction of OH with CO, C_2H_4, and C_2H_2. J Chem Soc Faraday Trans II 69:1617
55. Ravishankara AR, Thompson RL (1983) Kinetic study of the reaction of OH with CO from 250 to 1040 K. Chem Phys Lett 99:377
56. Forster R, Frost M, Fulle D, Hamann HF, Schlepegrell A, Troe J (1995) High pressure range of the addition of HO to HO, NO, NO_2, and CO. I. Saturated laser induced fluorescence measurements at 298 K. J Chem Phys 103:2949
57. Fulle D, Hamann HF, Hippler H, Troe J (1996) High pressure range of addition reactions of HO. II. Temperature and pressure dependence of the reaction $HO + CO <=> HOCO <=> H + CO_2$. J Chem Phys 105:983
58. Golden DM, Smith GP, McEwen AB, Yu C-L, Eiteneer B, Frenklach M, Vaghjiani GL, Ravishankara AR, Tully FP (1998) OH(OD) + CO: measurements and an optimized RRKM fit. J Phys Chem A 102:8598
59. Brunning J, Derbyshire DW, Smith IWM, Williams MD (1988) Kinetics of OH(v = 0,1) and OD(v = 0,1) with CO and the mechanism of the OH + CO reaction. J Chem Soc Faraday Trans II 84:105
60. Frost MJ, Sharkey P, Smith IWM (1993) Reaction between hydroxyl (deuteroxyl) radicals and carbon monoxide at temperatures down to 80 K: experiment and theory. J Phys Chem 97:12254
61. Spencer JE, Glass GP (1977) Some reactions of OH(v = 1). Int J Chem Kinet 9:111
62. Kohno N, Izumi M, Kohguchi H, Yamasaki K (2011) Acceleration of the reaction $OH + CO \rightarrow H + CO_2$ by vibrational excitation of OH. J Phys Chem A 115:4867
63. Zhu RS, Diau EGW, Lin MC, Mebel AM (2001) A computational study of the OH(OD) + CO reactions: effects of pressure, temperature, and quantum-mechanical tunneling on product formation. J Phys Chem A 105:11249
64. Senosian JP, Klippenstein SJ, Miller JA (2005) A complete statistical analysis of the reaction between OH and CO. Proc Combus Inst 30:945
65. Chen W-C, Marcus RA (2005) On the theory of the CO + OH reaction, included H and C kinetic isotope effects. J Chem Phys 123:094307
66. Nguyen TL, Xue BC, Weston RE Jr, Barker JR, Stanton JF (2012) Reaction of HO with CO: tunneling Is Indeed Important. J Phys Chem Lett 3:1549
67. Guo H (2012) Quantum dynamics of complex-forming bimolecular reactions. Int Rev Phys Chem 31:1
68. Schatz GC, Fitzcharles MS, Harding LB (1987) State-to-state chemistry with fast hydrogen atoms. Faraday Disc Chem Soc 84:359

69. Yu H-G, Muckerman JT, Sears TJ (2001) A theoretical study of the potential energy surface for the reaction $OH + CO \rightarrow H + CO_2$. Chem Phys Lett 349:547
70. Lakin MJ, Troya D, Schatz GC, Harding LB (2003) A quasiclassical trajectory study of the reaction $OH + CO \rightarrow H + CO_2$. J Chem Phys 119:5848
71. Valero R, Van Hemert MC, Kroes G-J (2004) Classical trajectory study of the HOCO system using a new interpolated ab initio potential energy surface. Chem Phys Lett 393:236
72. Kudla K, Schatz GC (1991) A quasiclassical trajectory study of $H + CO_2 \rightarrow OH + CO$: bulk reaction dynamics and the effect of van der Waals precursor formation. J Phys Chem 95:8267
73. Kudla K, Schatz GC, Wagner AF (1991) A quasiclassical trajectory study of the $OH + CO$ reaction. J Chem Phys 95:1635
74. Kudla K, Koures A, Harding LB, Schatz GC (1992) A quasiclassical trajectory study of OH rotational excitation in $OH + CO$ collisions using ab initio potential surfaces. J Chem Phys 96:7465
75. Kudla K, Schatz GC (1995) Product state distributions in chemical reactions: the reaction $OH+CO \rightarrow H+CO_2$. In: Liu K, Wagner AF (eds) The chemical dynamics and kinetics of small radicals. World Scientific, Singapore, p 438
76. Bradley KS, Schatz GC (1997) A quasiclassical trajectory study of $H + CO_2$: angular and translational distributions and OH angular momentum alignment. J Chem Phys 106:8464
77. Troya D, Lakin MJ, Schatz GC, Harding LB, Gonzalez M (2002) Quasiclassical trajectory study of energy and angular distributions for the $H + CO_2 \rightarrow OH + CO$ reaction. J Phys Chem B 106:8148
78. Garcia E, Saracibar A, Zuazo L, Lagana A (2007) A detailed trajectory study of the $OH + CO \rightarrow H + CO_2$ reaction. Chem Phys 332:162
79. Garcia E, Corchado JC, Espinosa-García J (2012) A detailed product distribution analysis of some potential energy surfaces describing the $OH + CO \rightarrow H + CO_2$ reaction. Comput Theor Chem 990:47
80. Laganà A, Garcia E, Paladini A, Casavecchia P, Balucani N (2012) The last mile of molecular reaction dynamics virtual experiments: the case of the $OH(N = 1–10) + CO(j = 0–3)$ reaction. Faraday Disc 157:415
81. Valero R, Andersson S (2012) Quantitative integral cross sections for the $H + CO_2 \rightarrow OH + CO$ reaction from a density functional theory-based potential energy surface. Phys Chem Chem Phys 14:16699
82. Schatz GC, Dyck J (1992) A reduced dimension quantum reactive scattering study of $OH + CO \rightarrow H + CO_2$. Chem Phys Lett 188:11
83. Clary DC, Schatz GC (1993) Quantum and quasiclassical calculations on the $OH + CO \rightarrow CO_2 + H$ reaction. J Chem Phys 99:4578
84. Hernandez MI, Clary DC (1994) Study of HOCO resonances in the $OH–CO \rightarrow CO_2 + H$ reaction. J Chem Phys 101:2779
85. Zhang DH, Zhang JZH (1995) Quantum calculations of reaction probabilities for $HO + CO \rightarrow H + CO_2$ and bound states of HOCO. J Chem Phys 103:6512
86. Goldfield EM, Gray SK, Schatz GC (1995) Quantum dynamics of a planar model for the complex forming $OH + CO \rightarrow H + CO_2$ reaction. J Chem Phys 102:8807
87. Dzegilenko F, Bowman JM (1996) Recovering a full dimensional quantum rate constant from a reduced dimensionality calculation: application to the $OH + CO \rightarrow H + CO_2$ reaction. J Chem Phys 105:2280
88. Dzegilenko F, Bowman JM (1998) "Spectator" modes in resonance-driven reactions: three-dimensional quantum calculations of HOCO resonances. J Chem Phys 108:511
89. McCormack DA, Kroes G-J (2002) Converged five-dimensional quantum calculations for $OH + CO \rightarrow H + CO_2$. J Chem Phys 116:4184
90. McCormack DA, Kroes G-J (2002) Full-dimensional quantal initial state-selected reaction probabilities $(J = 0)$ for the reaction $OH(v = 0,\ j = 0) + CO(v = 0,\ j = 0) \rightarrow CO_2 + H$. Chem Phys Lett 352:281
91. Medvedev DM, Gray SK, Goldfield EM, Lakin MJ, Troya D, Schatz GC (2004) Quantum wave packet and quasiclassical trajectory studies of $OH + CO$: influence of the reactant channel well on thermal rate constants. J Chem Phys 120:1231

92. He Y, Goldfield EM, Gray SK (2004) Quantum dynamics of vibrationally activated OH–CO reactant complexes. J Chem Phys 121:823
93. Valero R, McCormack DA, Kroes G-J (2004) New results for the OH(v = 0, j = 0) + CO(v = 0, j = 0) → H + CO_2 reaction: five and full-dimensional quantum dynamical study on several potential energy surfaces. J Chem Phys 120:4263
94. Valero R, Kroes G-J (2004) Theoretical reaction dynamics study of the effect of vibrational excitation of CO on the OH + CO → H + CO_2 reaction. J Phys Chem A 108:8672
95. Valero R, Kroes G-J (2004) Role of CO vibration in the complex-forming OH + CO → H + CO_2 reaction. Phys Rev A 70:040701
96. Valero R, Kroes G-J (2006) Identifying spectator bonds in modeling reactions: OH + CO → H + CO_2. Chem Phys Lett 417:43
97. Liu S, Xu X, Zhang DH (2011) Communication: state-to-state quantum dynamics study of the OH + CO → H + CO_2 reaction in full dimensions (J = 0). J Chem Phys 135:141108
98. Liu S, Xu X, Zhang DH (2012) A full-dimensional time-dependent wave packet study of the OH + CO → H + CO_2 reaction. Theor Chem Acc 131:1068
99. Wang C, Liu S, Zhang DH (2012) Effects of reagent vibrational excitation on the state-to-state quantum dynamics of the OH + CO → H + CO_2 reaction in six dimensions (J = 0). Chem Phys Lett 537:16
100. Li J, Wang Y, Jiang B, Ma J, Dawes R, Xie D, Bowman JM, Guo H (2012) Communication: a chemically accurate global potential energy surface for the HO + CO → H + CO_2 reaction. J Chem Phys 136:041103
101. Li J, Xie C, Ma J, Wang Y, Dawes R, Xie D, Bowman JM, Guo H (2012) Quasi-classical dynamics of the HO + CO → H + CO_2 reaction on a new ab initio based potential energy surface. J Phys Chem A 116:5057
102. Xie C, Li J, Xie D, Guo H (2012) Quasi-classical trajectory study of the H + CO_2 → HO + CO reaction on a new ab initio based potential energy surface. J Chem Phys 127:024308
103. Shiozaki T, Werner H-J (2013) Multireference explicitly correlated F12 theories. Mol Phys 111:607
104. Braams BJ, Bowman JM (2009) Permutationally invariant potential energy surfaces in high dimensionality. Int Rev Phys Chem 28:577
105. Bowman JM, Czakó G, Fu B (2011) High-dimensional ab initio potential energy surfaces for reaction dynamics calculations. Phys Chem Chem Phys 13:8094
106. Lester MI, Pond BV, Anderson DT, Harding LB, Wagner AF (2000) Exploring the OH + CO reaction coordinate via infrared spectroscopy of the OH–CO reactant complex. J Chem Phys 113:9889
107. Ma J, Li J, Guo H (2012) Quantum dynamics of the HO + CO → H + CO_2 reaction on an accurate potential energy surface. J Phys Chem Lett 3:2482
108. Lin SY, Guo H (2003) Quantum wave packet study of reactive and inelastic scattering between C(^{1}D) and H_2. J Chem Phys 119:11602
109. Alagia M, Balucani N, Casavecchia P, Stranges D, Volpi GG (1993) Crossed beam studies of four-atom reactions: the dynamics of OH + CO. J Chem Phys 98:8341
110. Brouard M, Hughes DW, Kalogerakis KS, Simons JP (2000) The product rovibrational and spin–orbit state dependent dynamics of the complex reaction H + CO_2 → OH + CO: memories of a lifetime. J Chem Phys 112:4557
111. Bowman JM (1991) Reduced dimensionality theory of quantum reactive scattering. J Phys Chem 95:4960
112. Corchado JC, Espinosa-Garcia J, Li J, Guo H (2013) CO_2 vibrational state distributions from quasi-classical trajectory studies of the HO + CO → H + CO_2 reaction and H + CO_2 inelastic collision. J Phys Chem A 117:11648
113. Frost MJ, Salh JS, Smith IWM (1991) Vibrational-state distribution of CO_2 produced in the reaction between OH radicals and CO. J Chem Soc Faraday Trans 87:1037
114. Casavecchia P, Balucani N, Volpi GG (1995) Reactive scattering of O(^{3}P, ^{1}D), Cl(^{2}P) and OH radicals. In: Wagner AF, Liu K (eds) Chemical dynamics and kinetics of small free radicals, vol Part I. World Scientific, Singapore, p 365

115. Nickolaisen SL, Cartland HE, Wittig C (1992) CO internal excitation from the reaction: $H + CO_2 \rightarrow CO + OH$. J Chem Phys 96:4378
116. Rice JK, Baronavski AP (1991) Nonstatistical CO product distributions from the hot H-atom reaction, $H + CO_2 \rightarrow OH + CO$. J Chem Phys 94:1006
117. Baulch DL, Bowman CT, Cobos CJ, Cox RA, Just T, Kerr JA, Pilling MJ, Stocker D, Troe J, Tsang W et al (2005) Evaluated kinetic data for combustion modeling: supplement II. J Phys Chem Ref Data 34:757
118. Jacobs A, Wahl M, Weller R, Wolfrum J (1989) Absolute reactive cross section and oh product state distribution for the reaction H(1.86 eV) $+ CO_2 \rightarrow OH + CO$. Chem Phys Lett 158:161
119. Hoffmann G, Oh D, Chen Y, Engel YM, Wittig C (1990) Photoinitiated reactions of H atoms with CO_2: OH(v = 0) rotational excitation from the 239 nm photolysis of CO_2HI complexes. Israel J Chem 30:115
120. Chen J, Xu X, Xu X, Zhang DH (2013) Communication: an accurate global potential energy surface for the $OH + CO \rightarrow H + CO_2$ reaction using neural networks. J Chem Phys 138:221104
121. Neumark DM (2006) Probing chemical dynamics with negative ions. J Chem Phys 125:132303
122. Zhang DH, Yang M, Collins MA, Lee S-Y (2002) Probing the transition state via photoelectron and photodetachment spectroscopy of H_3O^-. Proc Natl Acad Sci U S A 99:11579
123. Clements TG, Continetti RE, Francisco JS (2002) Exploring the $OH + CO \rightarrow H + CO_2$ potential surface via dissociative photodetachment of $(HOCO)^-$. J Chem Phys 117:6478
124. Lu Z, Hu Q, Oakman JE, Continetti RE (2007) Dynamics on the HOCO potential energy surface studied by dissociative photodetachment of $HOCO^-$ and $DOCO^-$. J Chem Phys 126:194305
125. Lu Z, Oakman JE, Hu Q, Continetti RE (2008) Photoelectron–photofragment angular correlations in the dissociative photodetachment of $HOCO^-$. Mol Phys 106:595
126. Johnson CJ, Continetti RE (1895) Dissociative photodetachment studies of the cooled $HOCO^-$ anions revealing dissociation below the barrier to $H + CO_2$. J Phys Chem Lett 2010:1
127. Johnson CJ, Poad BLJ, Shen BB, Continetti RE (2011) Communication: new insight into the barrier governing CO_2 formation from OH + CO. J Chem Phys 134:171106
128. Johnson CJ, Harding ME, Poad BLJ, Stanton JF, Continetti RE (2011) Electron affinities, well depths, and vibrational spectroscopy of cis- and trans-HOCO. J Am Chem Soc 133:19606
129. Zhang S, Medvedev DM, Goldfield EM, Gray SK (2006) Quantum dynamics study of the dissociative photodetachment of $HOCO^-$. J Chem Phys 125:164312
130. Ma J, Li J, Guo H (2012) Tunneling facilitated dissociation to $H + CO_2$ in $HOCO^-$ photodetachment. Phys Rev Lett 109:063202
131. Schreiner PR, Reisenauer HP, Pickard F IV, Simmonett AC, Allen WD, Matyus E, Csaszar AG (2008) Capture of hydroxymethylene and its fast disappearance through tunneling. Nature 453:906
132. Schreiner PR, Reisenauer HP, Ley D, Gerbig D, Wu C-H, Allen WD (2011) Methylhydroxycarbene: tunneling control of a chemical reaction. Science 332:1300